Journal of Molecular Liquids 210 (2015) 264–271

Contents lists available at ScienceDirect

Journal of Molecular Liquids

journal homepage: www.elsevier.com/locate/molliq

Comprehensive study on the impact of the cation alkyl side chain length on the solubility of water in ionic liquids

Kiki A. Kurnia [a], Catarina M.S.S. Neves [a], Mara G. Freire [a], Luís M.N.B.F. Santos [b], João A.P. Coutinho [a,*]

[a] Departamento de Química, CICECO, Universidade de Aveiro, 3810-193 Aveiro, Portugal
[b] Centro de Investigação em Química, Departamento de Química e Bioquímica, Faculdade de Ciências da Universidade do Porto, R. Campo Alegre 687, P-4169-007 Porto, Portugal

ARTICLE INFO

Article history:
Received 13 January 2015
Received in revised form 20 March 2015
Accepted 23 March 2015
Available online 28 March 2015

Keywords:
Water solubility
Ionic liquid
Imidazolium-based
Trend shift
Symmetry
Asymmetry
COSMO-RS
Ab initio

ABSTRACT

A comprehensive study on the phase behaviour of two sets of ionic liquids (ILs) and their interactions with water is here presented through combining experimental and theoretical approaches. The impact of the alkyl side chain length and the cation symmetry on the water solubility in the asymmetric $[C_{N-1}C_1im][NTf_2]$ and symmetric $[C_{N-1}C_{N-1}im][NTf_2]$ series of ILs (N up to 22), from 288.15 K to 318.15 K and at atmospheric pressure, was studied. The experimental data reveal that the solubility of water in ILs with an asymmetric cation is higher than in those with the symmetric isomer. Several trend shifts on the water solubility as a function of the alkyl side chain length were identified, namely at $[C_6C_1im][NTf_2]$ for asymmetric ILs and at $[C_4C_4im][NTf_2]$ and $[C_7C_7im][NTf_2]$ for the symmetric ILs. To complement the experimental data and to further investigate the molecular-level mechanisms behind the dissolution process, density functional theory calculations, using the Conductor-like Screening Model for Real Solvents (COSMO-RS) and the electrostatic potential-derived CHelpG, were performed. The COSMO-RS model is able to qualitatively predict water solubility as a function of temperature and alkyl chain lengths of both symmetric and asymmetric cations. Furthermore, the model is also capable to predict the somewhat higher water solubility in the asymmetric cation, as well as the trend shift as a function of alkyl chain lengths experimentally observed. Both COSMO-RS and the electrostatic potential-derived CHelpG show that the interactions of water and the IL cation take place on the IL polar region, namely on the aromatic head and adjacent methylene groups that explains the differences in water solubility observed for cations with different chain lengths. Furthermore, the CHelpG calculations for the isolated cations in the gas phase indicates that the trend shift of water solubility as a function of alkyl chain lengths and the difference of water solubility in symmetric may also result from the partial positive charge distribution/contribution of the cation.

1. Introduction

Ionic liquids (ILs) are low melting temperature organic salts which due to their ionic nature present outstanding properties that contributed to their common epithet as "green solvents" [1]. As a result, ILs have known increasing interest from both academia and industry as replacements for toxic and volatile organic solvents that are currently used in diverse industrial processes [2]. One of the most attractive features of ILs results from the possibility of tuning their properties by an appropriate selection of cation and anion, making of them "designer solvents" [3]. A large amount of experimental and theoretical contributions in the IL field has been reported in the last decade, and led researchers to an era where general theories need to be developed to systematically explain and predict the IL phase behaviour based on their interactions with other species, rather than just studying individual ILs and isolated mixtures. A unified understanding allows researchers to systematically design ILs for target applications. A main point that needs to be highlighted in order to design ILs is to make a link between the fundamental properties, such as electronic and molecular structure, and specific macromolecular physical and chemical properties.

The study of ILs in our research group has been focused on this direction by combining both experimental and computational approaches. This work represents an extension of our contribution towards the understanding of the relationship between the hydrophobic IL chemical structures and their impact on their mutual solubilities with water [4–12]. Here, we focus on hydrophobic ILs, which are promising media for liquid–liquid extractions from aqueous solutions [13–15]. The effects of various IL structural characteristics, namely the IL anion nature [4,5], cation head group [4,6,7], cation alkyl side chain length [8], structural/positional isomers [9,10], and fluorinated moieties [11], on their phase behaviour with water have been previously reported. From these works [4–12], and in terms of IL–water interactions, the IL structural features can be summarized as follows: (*i*) the anion plays a dominant role, that is, the higher the hydrogen bond basicity of the anion the more intense its interaction with water [4,5,9]; and (*ii*) the cation head and the cation alkyl side chain length have a significant although minor contribution [4,6,8,10,12]. In addition, all these systems showed

* Corresponding author.
E-mail address: jcoutinho@ua.pt (J.A.P. Coutinho).

http://dx.doi.org/10.1016/j.molliq.2015.03.040
0167-7322/

an upper critical solution temperature (UCST) behaviour, in which the UCST increases with the cation alkyl side chain length [4–12]. However, it should be noted that some IL–water mixtures present lower critical solution temperature (LCST) behaviour [16,17].

Although the contributions by us [4–12] and others [16–22] provided considerable information regarding the structural variation of ILs and its impact on their mutual solubilities with water, it is still a challenge to understand these ionic compounds at the molecular level. Herein, we investigated the solubility of water in a set of asymmetric $[C_{N-1}C_1im][NTf_2]$ and symmetric $[C_{N-1}C_{N-1}im][NTf_2]$ ILs (N up to 22), from 288.15 K to 318.15 K and at atmospheric pressure, aiming at addressing the impact of the cation alkyl chain length and the cation symmetry on this property. The symmetry of the cation provides a different structural organization which can be used to tune the physical properties of IL [23–30] and, ultimately, contribute to better design of ILs for a given task. To complement the experimental data, additional quantum chemical density functional theory (DFT) calculations were carried out, *via* computational simulations, namely by the COnductor-like Screening Model for Real Systems (COSMO-RS) [31] and electrostatic potential-derived CHelpG [32]. Theoretical calculations can compensate some shortcomings of the experiments and provide information on the relationship between the IL electronic/chemical structures and their mutual solubilities with water. In this way, the investigations based on the electronic level provide a more direct understanding on the intra- and intermolecular interactions.

2. Materials and methods

2.1. Chemicals and apparatus

The water solubility, from (288.15 to 318.15) K and at atmospheric pressure, was measured in nine ILs with the common bis(trifluoromethylsulfonyl)imide anion, $[NTf_2]^-$, combined with the following cations: 1-methyl-3-nonylimidazolium, $[C_9C_1im][NTf_2]$; 1-decyl-3-methylimidazolium, $[C_{10}C_1im][NTf_2]$; 1-methyl-3-undecylimidazolium, $[C_{11}C_1im][NTf_2]$; 1,3-dihexylimidazolium, $[C_6C_6im][NTf_2]$; 1,3-diheptylimidazolium, $[C_7C_7im][NTf_2]$; 1,3-dioctylimidazolium, $[C_8C_8im][NTf_2]$; 1,3-dinonylimidazolium, $[C_9C_9im][NTf_2]$; 1,3-didecylimidazolium, $[C_{10}C_{10}im][NTf_2]$; and 1,3-diundecylimidazolium, $[C_{11}C_{11}im][NTf_2]$. The general chemical structures of the studied ILs are given in Fig. 1. All of the ILs were purchased from Iolitec with a purity level >99 wt.%. Prior to the measurements, the ILs were carefully degassed and dried to remove small traces of impurities, by subjecting them to vacuum (0.1 Pa), at a moderate temperature (313.15 K) and under constant stirring for at least 48 h. After this procedure, the purity of each IL was further confirmed by ^1H, ^{13}C and ^{19}F NMR spectroscopy (Bruker Avance 300 MHz NMR spectrometer) using the d_6-DMSO solvent and tetramethylsilane as the internal standard. The water content of the dried ILs, as well as in IL-rich phase samples, was determined by a Metrohm 831 Karl Fisher (KF) coulometer, using the analyte Hydranal® — Coulomat AG from Riedel-de Haën. Throughout the experiments, ultrapure water (double distilled, passed by a reverse osmosis system, and further treated with a MilliQ plus 185 water purification equipment) was used. It presents a resistivity of 18.2 MΩ cm, a total organic carbon smaller than 5 $\mu g \cdot dm^{-3}$ and is free of particles >0.22 μm.

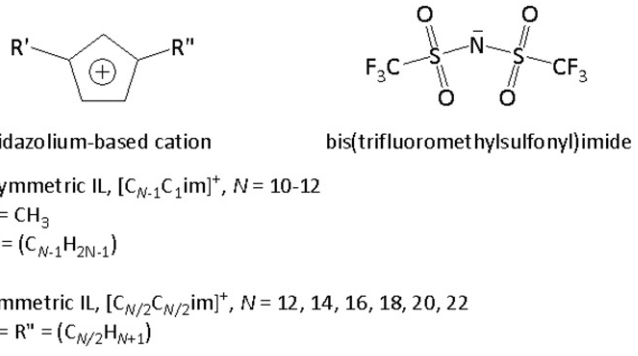

Fig. 1. Chemical structure of the imidazolium-based ILs investigated, where N corresponds to the total number of carbons in the two alkyl side chains of the cation.

2.2. Water solubility in ILs

All experiments to determine the solubility of water in the diverse ILs were conducted using the analytical method reported in our previous studies [4–6,8–12]. Briefly, samples of IL–water binary mixtures are placed in tightly-closed glass vials with a septum cap. The samples are then vigorously stirred and allowed to settle and equilibrate inside an aluminium block, specially designed for the purpose and able to maintain the temperature of interest, for at least 72 h. This period of time proved to be enough to guarantee a complete separation of the two phases, as well as their mutual saturation [9]. The aluminium block is further placed in an isolated air bath capable of maintaining the temperature within ±0.01 K. The temperature control is achieved with a PID temperature controller driven by a calibrated Pt100 (class 1/10) temperature sensor inserted in the aluminium block. A Julabo (model F25-HD) refrigerated bath and circulator is used as the cooling source.

The water content in the IL-rich phase was determined by Karl Fisher (KF) titration, using a Metrohm 831 coulometer. In this method, the IL-rich phase is sampled at each temperature from the equilibrium vials, using a glass syringe kept dry and at the same temperature of the measurements, and directly injected in the KF coulometric titrator. The quantification was performed gravimetrically within $\pm 10^{-4}$ g. For each sample and at a specific temperature, at least five individual measurements were carried out, allowing the determination of an average solubility value as well as the associated standard deviation.

2.3. COSMO-RS

COSMO-RS is a well-known predictive method developed by Klamt and co-workers [31,33] able to provide the thermodynamic properties and equilibrium of pure fluids and mixtures. It uses a statistical thermodynamic approach based on the results of unimolecular quantum chemical calculations. The detailed theory regarding COSMO-RS can be found in the original work of Klamt [31]. The advantage of using COSMO-RS is that the model not only can predict the properties of pure ILs and the phase behaviour of binary mixtures containing ILs, but also can give indications on the underlying molecular-level mechanisms [34,35].

The standard procedure of COSMO-RS calculations employed in this work consisted essentially in two major steps. First, the continuum solvation COSMO calculations of electronic density and molecular geometry of isolated water, cation, and anion were performed with the TURBOMOLE 6.1 program package on the density functional theory (DFT) level, utilizing the BP functional B88-P86 with a triple-ζ valence polarized basis set (TZVP) and the resolution of identity standard (RI) approximation [36]. All the optimized structures were confirmed to be minima on potential energy surface *via* vibrational frequency analysis. The absence of imaginary or negative frequencies indicated that the structure is a global minimum [37]. Second, the estimation of the phase diagrams of binary mixtures of ILs and water was performed with the COSMO*thermX* program using the parameter file BP_TZVP_C20_0111 (COSMOlogic GmbH & Co. KG, Leverkusen, Germany) [38]. It should be highlighted that in a previous work [6], we have demonstrated the capability of several COSMO-RS parameterizations to estimate phase diagrams for binary mixtures involving ILs and it was found that the parameter file BP_TZVP_C20_0111 gives predictive results more closer to the experimental data. Hence, the parameter file BP_TZVP_C20_0111 was used in this work. In all calculations, the ILs were always treated as isolated ions at the quantum chemical

level. Moreover, in a previous work [39], the best predictions of the experimental data were obtained with the lowest energy conformations or with the global minimum for both cation and anion. Thus, in this work, the lowest energy conformations of all the species involved were used in the COSMO-RS calculations.

2.4. Partial charge and charge delocalization

The optimized geometries of isolated water, IL cation and IL anion in the gas phase obtained with TURBOMOLE 6.1 were used as starting structures and were further optimized using the TZVP basis set and non-local BP exchange/correlation functional as implemented in Gaussian 03 Rev D.02 [40]. The optimized geometry having the lowest energy and with the absence of imaginary or negative frequencies [37], was used as the global minimum for the subsequent calculations. Thereafter, on the obtained minima, atomic charges of the isolated cation composing the studied ILs were retrieved by electrostatic surface potential (ESP) fits, using the CHelpG algorithm [32] to the electron densities obtained at the BP_TZVP level of theory.

3. Results and discussion

The novel experimental solubility of water in the investigated ILs, and at temperatures from 288.15 K to 318.15 K, are reported in Table 1. Those in the water-rich phase were not measurable with the approach commonly used [8,10] since the saturation solubility data were not reproducible that might be attributed due to micelle formation by long alkyl chain compounds. In addition, the solubility of water in $[C_{10}C_{10}im][NTf_2]$ and $[C_{11}C_{11}im][NTf_2]$ was determined in a narrower temperature range since these compounds are solid below 308.15 K. From the results presented in Table 1 it is concluded that the water-saturated IL-rich phase has a significant concentration of water, for all ILs investigated, and in the order of 10^{-1} (mole fraction). This shows that, despite the "hydrophobic" nature commonly attributed to $[NTf_2]$-based ILs, they are actually quite hygroscopic. In addition, the solubility of water in the IL increases with temperature — an indicative of UCST behaviour.

The data in the form of *T*–*x* (temperature *versus* mole fraction of water) phase diagrams for each binary system investigated are depicted in Fig. 2. Both experimental results and COSMO-RS predictions are presented. At the IL-rich phase, the shape of the equilibrium curve is similar in all the investigated systems. In addition, the curve shifts closer to the origin, *i.e.* the water solubility in ILs decreases, as the IL cation alkyl chain length increases. This trend is indeed common to other ILs, *e.g.*, for imidazolium-based ILs composed of different anions, such as hexafluorophosphate, $[PF_6]^-$ [4]; and tetrafluoroborate, $[BF_4]^-$ [18,19]. In addition, the set of ILs investigated also allows comparing the water solubility in two isomers with the same total number of carbon atoms at the two aliphatic moieties: $[C_6C_6im][NTf_2]$ and $[C_{11}C_1im][NTf_2]$. It is here shown that water is more soluble in $[C_{11}C_1im][NTf_2]$ (the asymmetric IL), in agreement with our previous results [10].

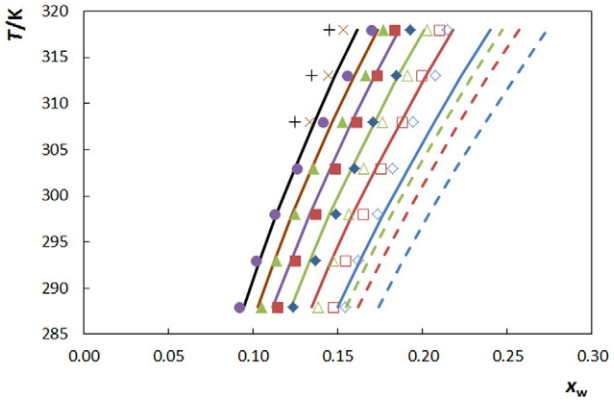

Fig. 2. Water solubility in ILs at several temperatures. Symbols: (♦,——), $[C_6C_6im][NTf_2]$; (■,——), $[C_7C_7im][NTf_2]$; (▲,——), $[C_8C_8im][NTf_2]$; (●,——), $[C_9C_9im][NTf_2]$; (×,——), $[C_{10}C_{10}im][NTf_2]$; (+,–), $[C_{11}C_{11}im][NTf_2]$; (◊,- - -), $[C_9C_1im][NTf_2]$; (□,- - -), $[C_{10}C_1im][NTf_2]$; and (△,- - -), $[C_{11}C_1im][NTf_2]$. The symbols and lines represent experimental data and COSMO-RS predictions, respectively.

Fig. 2 shows that the COSMO-RS model overestimates the mole fraction solubility of water in the studied ILs. Better agreement with the experimental data is obtained for the more "hydrophobic" ILs, *i.e.*, for those with longer alkyl side chains. This might result from an overestimation by the model of the hydrogen bond strength between water and the ILs [34,41]. Nevertheless, it should be highlighted that the COSMO-RS model is able to describe the decreasing saturation values of the solubility of water in ILs, and the increase of immiscibility gap, with increasing alkyl chain lengths experimentally observed. COSMO-RS is also able to predict higher solubility of water in the asymmetric ILs than its symmetric isomer. Furthermore, the dependence on temperature of the water solubility is also well-described by COSMO-RS, which means that the enthalpies of solution at the IL-rich phase are adequately predicted by the model. The main source of deviations between the predictions and the experimental data must thus rely on entropic effects inadequately described by the model.

Although it was not possible to experimentally determine the solubility of the investigated ILs in water, as mentioned previously, and based on the previous COSMO-RS satisfactory predictions, we can state that the solubility of these ILs in water varies between 2.33×10^{-5} for $[C_6C_6im][NTf_2]$ to 8.01×10^{-8} for $[C_{11}C_{11}im][NTf_2]$ (in mole fraction) at 298.15 K (*cf.* Table S1 in the Supporting information for detail prediction values). Therefore, the solubility of water in all the investigated ILs is several orders of magnitude higher than the solubility of ILs in water.

Assuming that in the temperature studied the molar enthalpy of solution of water in each IL can be considered temperature independent it

Table 1
Experimental mole fraction solubility of water (x_w) in ILs as a function of temperature and at 0.1 MPa along with the respective standard deviation, σ.

T/K	288.15	293.15	298.15	303.15	308.15	313.15	318.15
$(x_w \pm \sigma)$							
$[C_6C_6im][NTf_2]$	0.1233 ± 0.0003	0.1364 ± 0.0005	0.1489 ± 0.0004	0.1599 ± 0.0004	0.1708 ± 0.0006	0.1846 ± 0.0005	0.1929 ± 0.0007
$[C_7C_7im][NTf_2]$	0.1141 ± 0.0002	0.1247 ± 0.0004	0.1365 ± 0.0004	0.1484 ± 0.0003	0.1610 ± 0.0006	0.1727 ± 0.0005	0.1831 ± 0.0005
$[C_8C_8im][NTf_2]$	0.1046 ± 0.0003	0.1134 ± 0.0003	0.1246 ± 0.0002	0.1354 ± 0.0005	0.1527 ± 0.0005	0.1663 ± 0.0003	0.1769 ± 0.0002
$[C_9C_9im][NTf_2]$	0.0915 ± 0.0004	0.1016 ± 0.0004	0.1128 ± 0.0003	0.1257 ± 0.0004	0.1409 ± 0.0005	0.1551 ± 0.0006	0.1696 ± 0.0006
$[C_{10}C_{10}im][NTf_2]$					0.1337 ± 0.0005	0.1447 ± 0.0006	0.1532 ± 0.0006
$[C_{11}C_{11}im][NTf_2]$					0.1248 ± 0.0006	0.1343 ± 0.0006	0.1450 ± 0.0004
$[C_9C_1im][NTf_2]$	0.1542 ± 0.0003	0.1622 ± 0.0004	0.1736 ± 0.0003	0.1825 ± 0.0005	0.1946 ± 0.0005	0.2078 ± 0.0004	0.2148 ± 0.0004
$[C_{10}C_1im][NTf_2]$	0.1472 ± 0.0006	0.1545 ± 0.0005	0.1645 ± 0.0005	0.1754 ± 0.0006	0.1878 ± 0.0004	0.1992 ± 0.0004	0.2099 ± 0.0005
$[C_{11}C_1im][NTf_2]$	0.1383 ± 0.0005	0.1471 ± 0.0006	0.1567 ± 0.0006	0.1652 ± 0.0004	0.1761 ± 0.0004	0.1908 ± 0.0004	0.2026 ± 0.0005

is possible to use Eq. (1) to correlate the experimental water solubility data:

$$\ln x_w = A + \frac{B}{T/K} \quad (1)$$

where x_w is the mole fraction solubility of water in each IL, T is the absolute temperature, and A and B are correlation constants. The correlation constants obtained from the fitting are presented in Table 2. The good description of the experimental data by Eq. (1) is shown in Fig. S1 in the Supporting information. A maximum relative deviation from the experimental mole fraction data of 0.8% was observed. Due to the limited number of data points, Eq. (1) was not applied to the binary systems containing $[C_{10}C_{10}im][NTf_2]$ and $[C_{11}C_{11}im][NTf_2]$ (*cf.* Table 1).

It should be remarked that the solubility of water in all the studied ILs is well above what could be considered infinite dilution, and thus, without the activity coefficient of water, the associated molar thermodynamic functions of solution cannot be derived. Nonetheless, based on the slope obtained using Eq. (1) (*cf.* Table 2), which reflects the temperature dependence of the water solubility, some general remarks can be made. The dependence of the water solubility with temperature (shown in the Fig. S1 in Supporting information) is very similar to that obtained for the $[C_{N-1}C_1im][NTf_2]$ or $[C_{N/2}C_{N/2}im][NTf_2]$ with shorter alkyl side chains ($N < 10$) [8,10]. This similarity indicates that the cation alkyl side chain has a minor impact on the enthalpic interactions related with the water dissolution in ILs. In other word, the interaction of IL and water mostly occurs in the polar region of the respective ILs, in this case is the imidazolium head ring. Furthermore, the significantly more negative B values are indication of weaker (more positive) enthalpic of solvation in the symmetric series of ILs that reflects the balance between the change in the interaction and cavitation enthalpic contribution.

With a set of ILs with the same anion and cation head group, it is possible to investigate the origin of the differences in the water solubility resulting from the IL hydrophobicity induced by the increase of the alkyl chain length. To accomplish a more comprehensive study on this matter, the results obtained here were combined with those of our previous works [8,10] and are depicted in Fig. 3. At a fixed temperature (308.15 K), there is a decrease on the mole fraction solubility of water in ILs with the increase of the alkyl chain length for both symmetric and asymmetric series of ILs. Similar trends were observed at other temperatures as shown in Figs. S2–S3 in the Supporting information. Fig. 3 clearly shows that for the set of studied ILs, various regions and trend shifts can be observed as a function of the cation alkyl chain length, as previously remarked for various thermophysical properties [23–30]. The first region, here called "Region A", consists of the series of short alkyl chain length ILs with $N < 6$, and where the decrease (slope) on the mole fraction solubility of water is higher than that observed in "Region B". With the exception of $[C_1C_1im][NTf_2]$, both asymmetric and symmetric ILs in "Region A", display an average decrement of water solubility of 0.024 mole-fraction *per* methylene group (–CH_2–) addition at the cation. It should be mentioned that the higher capability of $[C_1C_1im][NTf_2]$ to dissolve a large amount of water (and being an outsider) might be explained by the change in the distribution and higher charge density of the cation, resulting from the sharp change in the inductive effect due to the change of the alkyl moieties by a "–CH_3" group in the imidazolium ring [26].

Table 2
Parameters for the correlation of the water solubility using Eq. (1) along with the corresponding standard deviation (σ) and the relative deviation from the fitting of the experimental solubility data.

IL	$(A \pm \sigma)$	$(B \pm \sigma)$/K	Relative deviation
$[C_6C_6im][NTf_2]$	2.67 ± 0.15	−1368 ± 45	0.01
$[C_7C_7im][NTf_2]$	2.92 ± 0.09	−1466 ± 27	0.01
$[C_8C_8im][NTf_2]$	3.51 ± 0.16	−1666 ± 49	0.01
$[C_9C_9im][NTf_2]$	4.24 ± 0.07	−1912 ± 21	0.01
$[C_9C_1im][NTf_2]$	1.77 ± 0.09	−1051 ± 28	0.01
$[C_{10}C_1im][NTf_2]$	1.95 ± 0.09	−1116 ± 26	0.01
$[C_{11}C_1im][NTf_2]$	2.06 ± 0.12	−1165 ± 37	0.01

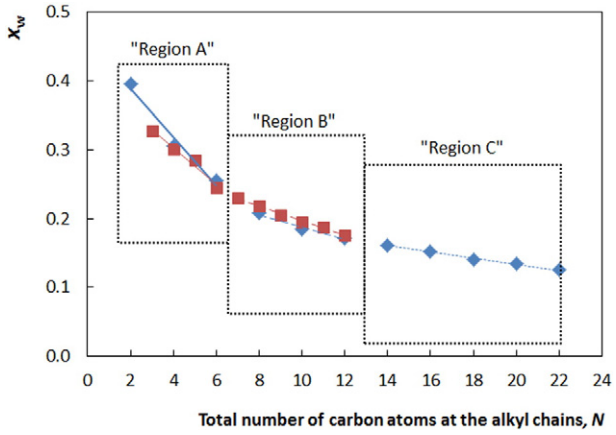

Fig. 3. Solubility of water in ILs, x_w, at $T = 308.15$ K and $p = 0.1$ MPa, as a function of the total number of carbon atoms at the alkyl chains, N: (♦) symmetric ILs and (■) asymmetric ILs. The lines are only presented to facilitate the reading and to better follow the trend shifts.

In "Region B", starting at $[C_6C_1im][NTf_2]$ or $[C_4C_4im][NTf_2]$, the mole fraction solubility of water shows a weaker dependence on the alkyl side chain length, with an average decrement on the mole fraction solubility of water of 0.008 for the symmetric and 0.011 for the asymmetric ILs *per* addition of –CH_2. Lastly, symmetric ILs with long alkyl chains, starting with $[C_7C_7im][NTf_2]$ in "Region C", show a very small decrement of 0.005 in the mole fraction solubility of water *per* methylene group. These results reveal that there are one trend shift in the mole fraction solubility of water observed at $[C_6C_1im][NTf_2]$ for the asymmetric series and two trend shifts at $[C_4C_4im][NTf_2]$ and $[C_7C_7im][NTf_2]$ for the symmetric ILs. These changes in the monotonically behaviour are related with the structural organization of the liquid above a critical alkyl chain length (CAL) and that is particularly emphasized by the cation structural isomerism with a higher symmetry ($[C_{N/2}C_{N/2}im][NTf_2]$ series) [23]. The change of the ionic liquid nanostructuration due to the change of alkyl chain length and structural isomerism has an impact in the solvation potential (cavitation and interaction). The higher dependence of the water solubility in the short alkyl chain length region "Region A" agrees with the preferential location (solvation) of the water molecules in the IL polar region in where the modification of the polar network and charge distribution is strongly affected by the alkyl chain size until the critical alkyl chain length (CAL). Above the CAL, "Region B" and "Region C" the decrease of the solubility is smoothed in agreement with minor change in charge distribution in the polar network region and the coexisting polar and nonpolar domains with a progressive bulkier nonpolar domains that can form a bicontinuous mesoscopic phase with a small change of the charge distribution associated with the more separate strands of the polar network. In this regard, in "Region B" and "Region C", increasing alkyl chain length of symmetric and asymmetric ILs, only lead to slight change of charge distribution on their respective imidazolium ring (as will be discussed in the following subsection), and consequently, indication to slight difference of water solubility as observed experimentally.

As mentioned before, similar trends were observed for the thermophysical properties of ILs, such as viscosity [23,24], surface tension [25], vapour pressures [26,27] and heat capacities [28] among others [29,30]. Although those studies focused on the physical properties of pure ILs with symmetric and asymmetric alkyl side chains, the two basic conclusions might also be extended to the water solubility on these series of ILs that are: (*i*) ILs are highly structured fluids with high-charge density areas permeated by low-charge density regions (the alkyl side chain); and (*ii*) the topology of the nonpolar domains is

strongly dependent on the relative volumes occupied by the polar and nonpolar moieties. Which means that, the interaction of water and ILs may take place on the high-charge density part of IL, that is the imidazolium ring. The steric hindrance stemming from the two alkyl side chains connected to the symmetric cations tends to separate the stacked imidazolium rings more than in the case of asymmetric cations. This may explain the slightly lower water solubility observed in the symmetric cations. Thus, aiming at a deeper understanding of the trend shifts observed in the IL–water phase behaviour, we performed additional quantum chemical calculations — discussed below.

3.1. COSMO-RS, partial charge, and charge delocalization

The interactions between IL ions and water molecules are closely related and derived from their electronic structure. A very powerful theoretical quantum chemical method, namely DFT, provides direct access to the electronic structures of a desired molecule. Therefore, in order to gather a detailed understanding on the impact of the cation alkyl chain length and further IL interactions with water, some systematic COSMO-RS and electrostatic potential-derived CHelpG studies were performed.

Concerning the COSMO-RS predictions, it was shown above that the model is able to predict saturation curves similar to those experimentally determined. In addition, despite its overestimation on the water solubility in ILs (*cf.* Fig. 2), the model is able to describe the decrease on the water solubility with the increase of the cation alkyl chain length and is even able to predict a higher water solubility in $[C_{11}C_1im][NTf_2]$ than in its symmetric isomer, $[C_6C_6im][NTf_2]$. Remarkably, COSMO-RS also predicts the trend shifts observed experimentally on the water solubility as a function of the total number of carbons at the cation alkyl side chains (*cf.* Fig. S4 in the Supporting information).

The satisfactory predictions obtained with COSMO-RS prompt us to further use this model, along with CHelpG analysis, to further delve into the mechanisms behind the water solvation in ILs. It should be mentioned, at this point, that a detailed discussion on the geometry and total energy of different conformers is beyond the scope of the present work. Here, we are restricted to the aspect directly related to the experimental findings. These results are discussed in terms of sigma profiles and potential, and atomic σ-moment (produced by COSMO-RS) and CHelpG charge distribution (calculated using Gaussian 03 Revision D.02). The coordinates, σ-moments, and CHelpG charges for all atoms are given in Tables S2 to Sx in the Supporting information. Additional details on the sigma profile and potential, atomic σ-moment, and CHelpG charge distribution can be found in the literature [31,40].

The sigma profile and potential of water are given in Fig. S5 in the Supporting information, whereas the sigma profile and potential of the IL cations and anions are given in Fig. 4. The key feature of the sigma profile is that when the screening charge density goes beyond $\pm 1.0\ e\cdot nm^{-2}$, the molecule is able to interact *via* hydrogen-bonding. The higher the charge density, the stronger IS the HB acceptor (+) or HB donor (−) characteristics of a given fluid. The sigma profile of water (*cf.* Fig. S5a) ranges from (2.2 to −1.9) $e\cdot nm^{-2}$. The peak at $1.8\ e\cdot nm^{-2}$ is assigned to the oxygen atom that acts as a hydrogen bond acceptor (HB_acc3 = 5.693), while the peak at $-1.6\ e\cdot nm^{-2}$ confirms its capability to act as a hydrogen bond donor (HB_don3 H_2O = 3.850). The electrostatic potentials of water, $[C_{11}C_1im]^+$, $[C_6C_6im]^+$, and $[NTf_2]^-$ are mapped in the isosurface as depicted in Fig. 5, where red and blue colours represent the negative and positive regions, respectively.

With the CHelpG electrostatic potential-derived charges determined for water (*cf.* Fig. 5a) it is further confirmed that the most electronegative regions are near the oxygen atom (−0.790) whereas the most electropositive ones are near the two hydrogen atoms (+0.395). Therefore, both the COSMO-RS and CHelpG charge distribution results are in agreement and essentially display the same quantum chemical information results.

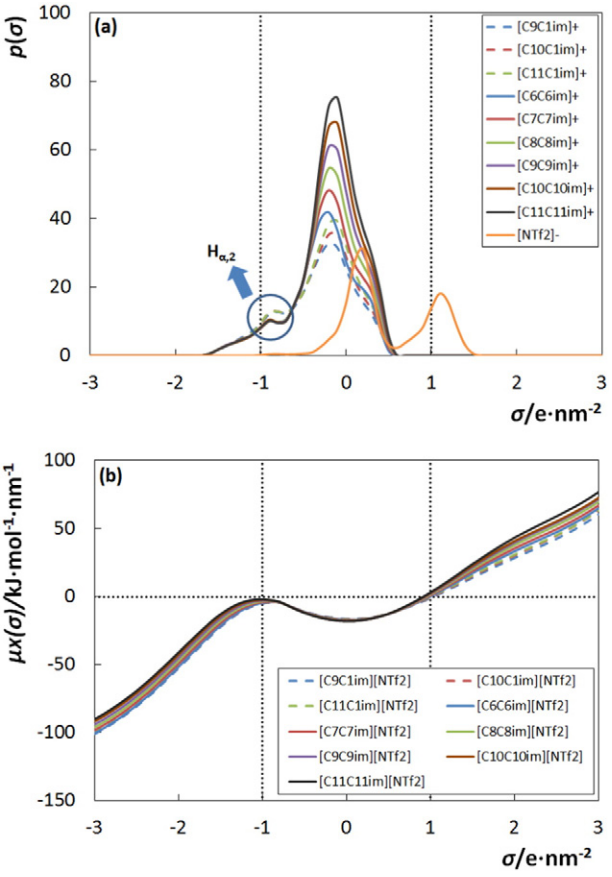

Fig. 4. Sigma profile (a) and potential (b) of IL cations and anions estimated using COSMO-RS at the BP_TZVP level.

In the studied set of ILs, having the same cation head core and anion, the differences in the water solubility values can be attributed to the cation alkyl chain length and these differences are here analysed. In addition, during the COSMO-RS and CHelpG calculations, we always used isolated IL ions that allow us to study their individual interactions with water molecules. The sigma profiles of the ILs indicate that the IL ions are either hydrogen bond donors or acceptors. For example, the sigma profile of $[NTf_2]^-$ anion ranges from (−0.4 to 1.5) $e\cdot nm^{-2}$, with peaks at 0.2 and 1.1 $e\cdot nm^{-2}$, and in which the latter peak indicates its ability to act as a weak HB-acceptor (HB_acc3 $[NTf_2]^-$ = 2.292). It should be remarked that according to the σ-moment, the HB_acc3 of $[NTf_2]^-$ arises from the central nitrogen and the four sulfonyl oxygen atoms (*cf.* Table S3 in the Supporting information). This evidence is further supported by the electrostatic potential surface (*cf.* Fig. 5d), where most regions in the ion are nearly neutral with the exception of the regions around the nitrogen and oxygen atoms. With respect to the CHelpG analysis, the partial atomic charge at the central nitrogen (−0.626) and the four oxygen (averaged charges = −0.500) atoms are negatives, while the negative charges on the fluorine atoms are not significant. Therefore, the four oxygen atoms and the central nitrogen atoms are the main regions of $[NTf_2]^-$ to interact *via* hydrogen bonding. These regions that possess negative electrostatic potential values are also those that mainly interact with the IL cation [6,42].

The sigma profiles for the IL cations range from (−1.6 to 0.6) $e\cdot nm^{-2}$ and are similar to each other. Two peaks are observed for the cation: (*i*) the first peak falls within the non-polar region and its intensity increases with the increase of the alkyl chain length; and (*ii*) the second peak, shoulder-alike and near the cut-off, at $-0.8\ e\cdot nm^{-2}$ (for the asymmetric cations) and $-0.9\ e\cdot nm^{-2}$ (for the symmetric cations), supports the weak hydrogen-bond donor ability of the studied IL

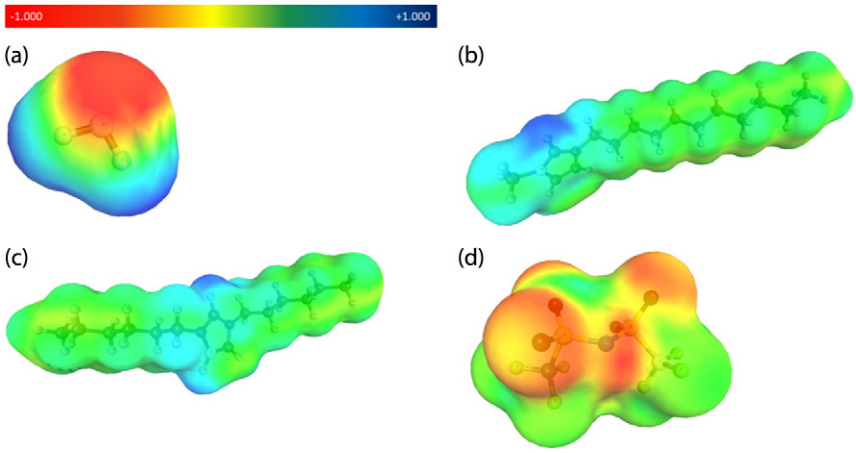

Fig. 5. Partial electrostatic potential-derived CHelpG charges distribution for optimized structures: (a) water, (b) $[C_{11}C_1im]^+$, (c) $[C_6C_6im]^+$, and (d) $[NTf_2]^-$ retrieved at the BP_TZVP level of theory. Complete pictures are given in the Supporting information.

cations. It is, however, interesting to note that, although having different alkyl chain lengths, the set of the studied asymmetric cations present identical peaks intensities at -0.8 e·nm^{-2} (*cf.* circled region in Fig. 4a) whereas the symmetric cations present identical peaks centred at -0.9 e·nm^{-2}. Furthermore, the asymmetric cation presents peaks with slightly higher intensity (*cf.* circled region in Fig. 4a) indicating their somewhat higher ability to hydrogen bond with water, and consequently higher solubility of water on them compare to the symmetric cation, as observed experimentally. This indication is further supported by the electrostatic potential surfaces of $[C_{11}C_1im]^+$ and $[C_6C_6im]^+$, as depicted in Fig. 5b and c, respectively (the other cations are not shown since they are similar).

The electrostatic potential of the cation is nearly neutral or weakly positive around the imidazolium ring. The CHelpG analysis shows that the double bond between C^4 and C^5 atoms (*cf.* Fig. 6 for the atomic labelling) and the other four electrons on the two N atoms are delocalized around the N_1–C_2–N_3 group. Based on our calculations, the higher positive charges in $H_{\alpha,2}$ support its more acidic character when compared to $H_{\alpha,4}$ and $H_{\alpha,5}$. This theoretical calculation is also supported by experimental data [43,44]. Furthermore, from the atomic σ-moment, it is evident that most of the positive charge of the cation is located within the imidazolium ring at the hydrogen atoms of the ionic headgroup (labelled as H_α in Fig. 6).

Experimental and theoretical studies have already shown that the main interactions which rule the solvation of water in ILs occur mainly between the IL anion and water [6,9,11,34,45–48]. From the above COSMO-RS and quantum chemical analyses, specific interactions between the IL ions and water exist between: (*i*) the $[NTf_2]^-$ with the hydrogen atoms of water; and (*ii*) the IL cation with the oxygen atoms of water. Since the studied ILs share the same cation head group and anion, the interaction strength with the water molecule might be determined by the effects derived from the different alkyl chain sizes in the IL structuration and charge distribution. Water is "solvated" preferentially in the polar regions and the amount of water soluble in the IL depends mainly in how the solvation potential of water in the IL polar network is affected by the change of the partial charge distribution [9]. For the asymmetric cation, the partial charges of H_α decrease considerably from $N = 2$ to $N = 6$, then reaches plateau up to $N = 12$. The partial positive charges of the symmetric cations also display a significant increase up to $N = 6$ and then reaches a plateau until $N = 22$. Remarkably, this trend shift on the partial positive charges of the cation is similar to that verified in the water solubility of the studied ILs remarkably follow the same trend to that verified in the water solubility. This suggests that in "Region A", the positive charge distribution/contribution of cation dominates their interaction with water. Meanwhile, in "Region B" (and "Region C" for the symmetric series), the positive charge distribution/contribution is similar (also further supported the peak on their sigma profile displayed in Fig. 4) leading to somehow similar hydrogen-bond ability explaining thus the change in

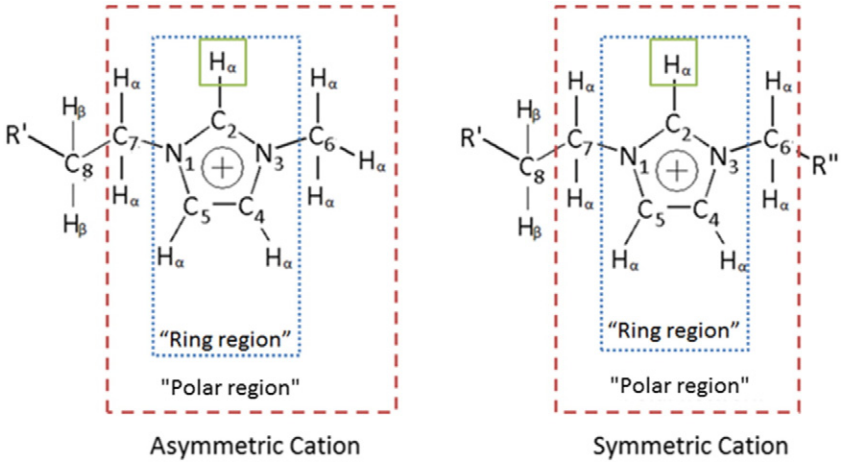

Fig. 6. Labelled structure of the imidazolium cation — similar to that used by Cremer et al. [49]. The most acidic hydrogen atom is attached to the C_2 carbon atom labelled as $H_{\alpha,2}$. Carbon atoms attached to the ring (C_2, C_4, and C_5) are labelled as "ring region". Carbon atoms attached to the ionic headgroup (C_2, C_4, C_5, C_6 and C_7) are labelled as "polar region".

slope of the decrease of solubility of water in ILs with the increasing cation chain length. The further decrease of water solubility with increasing alkyl chain lengths might result of less "free" space to accommodate water molecules around the "polar region".

The differences in the water solubility in the symmetric and asymmetric series of ILs can also be explained in the light of the partial positive charge distribution on their polar region. For example, the slightly higher water solubility in the asymmetric $[C_7C_1im][NTf_2]$, $[C_9C_1im][NTf_2]$ and $[C_{11}C_1im][NTf_2]$ when compared to its symmetric isomer, $[C_4C_4im][NTf_2]$, $[C_5C_5im][NTf_2]$ and $[C_6C_6im][NTf_2]$, respectively, results from the higher partial positive charge distribution on their respective cation. In this way, the symmetric cation contains a smaller amount H_α when compared to the asymmetric isomer. Furthermore, as previously mentioned, COSMO-RS results reveal that the asymmetric cation presents a shoulder-like peak with a slightly higher intensity when compared to the symmetric one (*cf.* Fig. 4c), and indicative of the higher capability of the former cation to serve as a hydrogen bond donor. It is argued that the lesser partial positive charge distribution of the symmetric cation, along with more bulky structures at two alkyl chains makes uneasy access to the high-charged region of symmetric cation, and consequently leading to low water solubility in the symmetric ILs.

4. Conclusions

In this comprehensive study through combining experimental and theoretical approaches, the water solubility in two series of asymmetric and symmetric ILs was investigated, aiming at understanding the impact of alkyl chain lengths and cation symmetry. In both series, the increase in temperature leads to increase of water solubility. The solubility of water decreases with increasing the cation alkyl side chain length for both asymmetric and symmetric ILs. Furthermore, one and two trend shifts, for the symmetric and asymmetric series of ILs, respectively, were observed on the water solubility as a function of the cation alkyl chain length.

COSMO-RS and electrostatic potential-derived CHelpG calculations were additionally used to gather a more complete scenario on the solvation of water in ILs. In regard to COSMO-RS, the model is able to qualitatively predict the impact of alkyl chain lengths and temperature towards water solubility on the set of studied ILs. Furthermore, COSMO-RS is also able to predict slightly higher water solubility in asymmetric cation and, remarkably, the trend shift of water solubility as a function of alkyl chain length as verified experimentally. The CHelpG calculation reveals that the observed trend shift might be related to the partial positive charge distribution of cation polar region. Furthermore, the difference of water solubility in symmetric and asymmetric isomer might also be addressed as the consequences of partial positive charge distribution/contribution of the respective cation.

Acknowledgement

This work was financed by national funding from the Fundação para a Ciência e a Tecnologia (FCT, Portugal), European Union, QREN, FEDER and COMPETE by the projects PEST-C/CTM/LA0011/2013 and PTDC/ACC-AMB/119172/2010. C.M.S.S. Neves and K.A. Kurnia also thank FCT for the doctoral SFRH/BD/70641/2010 and postdoctoral grants SFRH/BPD/88101/2012, respectively. M.G. Freire acknowledges the European Research Council (ERC) for the Grant ERC-2013-StG-337753.

Appendix A. Supplementary data

Supplementary data associated with this article can be found, in the online version, at http://dx.doi.org/10.1016/j.molliq.2015.03.040.

References

[1] P. Wasserscheid, T. Welton, Ionic Liquids in Synthesis, 2nd ed., vol. 1, Federal Republic of Germany: WILEY-VCH Verlag GmbH & Co. KGaA, Darmstadt, 2009.
[2] N.V. Plechkova, K.R. Seddon, Ionic Liquids Uncoiled — Critical Expert Overviews, A John Wiley & Sons, Inc., Publication, 2013.
[3] R.D. Rogers, Nature 447 (2007) 917–918.
[4] M.G. Freire, C.M.S.S. Neves, P.J. Carvalho, R.L. Gardas, A.M. Fernandes, I.M. Marrucho, L.M.N.B.F. Santos, J.A.P. Coutinho, J. Phys. Chem. B 111 (2007) 13082–13089.
[5] M.G. Freire, P.J. Carvalho, R.L. Gardas, L.M.N.B.F. Santos, I.M. Marrucho, J.A.P. Coutinho, J. Chem. Eng. Data 53 (2008) 2378–2382.
[6] K.A. Kurnia, T.E. Sintra, C.M.S.S. Neves, K. Shimizu, J.N. Canongia Lopes, F. Goncalves, S.P.M. Ventura, M.G. Freire, L.M.N.B.F. Santos, J.A.P. Coutinho, Phys. Chem. Chem. Phys. 16 (2014) 19952–19963.
[7] K.A. Kurnia, M.V. Quental, L.B. Santos, M.G. Freire, J.A.P. Coutinho, Phys. Chem. Chem. Phys. 17 (2015) 4569–4577.
[8] M.G. Freire, P.J. Carvalho, R.L. Gardas, I.M. Marrucho, L.M.N.B.F. Santos, J.A.P. Coutinho, J. Phys. Chem. B 112 (2008) 1604–1610.
[9] M.G. Freire, C.M.S.S. Neves, K. Shimizu, C.E.S. Bernardes, I.M. Marrucho, J.A.P. Coutinho, J.N. Canongia Lopes, L.P.N. Rebelo, J. Phys. Chem. B 114 (2010) 15925–15934.
[10] M.A.R. Martins, C.M.S.S. Neves, K.A. Kurnia, L. Andreia, L.M.N.B.F. Santos, M.G. Freire, S.P. Pinho, J.A.P. Coutinho, Fluid Phase Equilib. 375 (2014) 161–167.
[11] C.M.S.S. Neves, K.A. Kurnia, K. Shimizu, I.M. Marrucho, L.P.N. Rebelo, J.A.P. Coutinho, M.G. Freire, J.N. Canongia Lopes, Phys. Chem. Chem. Phys. 16 (2014) 21340–21348.
[12] M.A.R. Martins, C.M.S.S. Neves, K.A. Kurnia, L.M.N.B.F. Santos, M.G. Freire, S.P. Pinho, J.A.P. Coutinho, Fluid Phase Equilib. 381 (2014) 28–35.
[13] A. Chapeaux, L.D. Simoni, T.S. Ronan, M.A. Stadtherr, J.F. Brennecke, Green Chem. 10 (2008) 1301–1306.
[14] A.G. Fadeev, M.M. Meagher, Chem. Commun. (2001) 295–296.
[15] L.D. Simoni, A. Chapeaux, J.F. Brennecke, M.A. Stadtherr, Comput. Chem. Eng. 34 (2010) 1406–1412.
[16] Y. Kohno, H. Ohno, Chem. Commun. 48 (2012) 7119–7130.
[17] K. Fukumoto, H. Ohno, Angew. Chem. Int. Ed. 46 (2007) 1852–1855.
[18] F.M. Maia, O. Rodríguez, E.A. Macedo, Fluid Phase Equilib. 296 (2010) 184–191.
[19] F.M. Maia, O. Rodríguez, E.A. Macedo, J. Chem. Thermodyn. 48 (2012) 221–228.
[20] F.M. Maia, O. Rodríguez, E.A. Macedo, Ind. Eng. Chem. Res. 51 (2012) 8061–8068.
[21] T. Zhou, L. Chen, Y. Ye, Z. Qi, H. Freund, K. Sundmacher, Ind. Eng. Chem. Res. 51 (2012) 6256–6264.
[22] M.G. Freire, L.M.N.B.F. Santos, A.M. Fernandes, J.A.P. Coutinho, I.M. Marrucho, Fluid Phase Equilib. 261 (2007) 449–454.
[23] M.A.A. Rocha, C.M.S.S. Neves, M.G. Freire, O. Russina, A. Triolo, J.A.P. Coutinho, L.M.N.B.F. Santos, J. Phys. Chem. B 117 (2013) 10889–10897.
[24] M.A.A. Rocha, F.M.S. Ribeiro, A.I.M.C.L. Ferreira, J.A.P. Coutinho, L.M.N.B.F. Santos, J. Mol. Liq. 188 (2013) 196–202.
[25] H.F.D. Almeida, M.G. Freire, A.M. Fernandes, J.A. Lopes-Da-Silva, P. Morgado, K. Shimizu, E.J.M. Filipe, J.N. Canongia Lopes, L.M.N.B.F. Santos, J.A.P. Coutinho, Langmuir 30 (2014) 6408–6418.
[26] M.A.A. Rocha, C.F.R.A.C. Lima, L.R. Gomes, B. Schröder, J.A.P. Coutinho, I.M. Marrucho, J.M.S.S. Esperança, L.P.N. Rebelo, K. Shimizu, J.N.C. Lopes, L.M.N.B.F. Santos, J. Phys. Chem. B 115 (2011) 10919–10926.
[27] M.A.A. Rocha, J.A.P. Coutinho, L.M.N.B.F. Santos, J. Chem. Phys. 141 (2014).
[28] M.A.A. Rocha, M. Bastos, J.A.P. Coutinho, L.M.N.B.F. Santos, J. Chem. Thermodyn. 53 (2012) 140–143.
[29] M.A.A. Rocha, J.A.P. Coutinho, L.M.N.B.F. Santos, J. Phys. Chem. B 116 (2012) 10922–10927.
[30] M.A.A. Rocha, J.A.P. Coutinho, L.M.N.B.F. Santos, J. Chem. Phys. 139 (2013).
[31] A. Klamt, COSMO-RS From Quantum Chemistry to Fluid Phase Thermodynamics and Drug Design, Elsevier, Amsterdam, The Netherlands, 2005.
[32] C.M. Breneman, K.B. Wiberg, J. Comput. Chem. 11 (1990) 361–373.
[33] A. Klamt, F. Eckert, Fluid Phase Equilib. 172 (2000) 43–72.
[34] K.A. Kurnia, J.A.P. Coutinho, Ind. Eng. Chem. Res. 52 (2013) 13862–13874.
[35] J.F.B. Pereira, K.A. Kurnia, O.A. Cojocaru, G. Gurau, L.P.N. Rebelo, R.D. Rogers, M.G. Freire, J.A.P. Coutinho, Phys. Chem. Chem. Phys. 16 (2014) 5723–5731.
[36] University of Karlsruhe, Forschungszentrum Karlsruhe GmbH, TURBOMOLE V6.1 2009, 1989–2007, 25 GmbH, Since 2007available from http://www.turbomole.com.
[37] J.B. Foresma, A. Frisch, Exploring Chemistry With Electronic Structure Methods, 2nd ed. Gaussian Inc., Pittsburgh, 1996.
[38] F. Eckert, A. Klamt, COSMOtherm Version C2.1 Release 01.08, COSMOlogic GmbH & Co. KG, Leverkusen, Germany, 2006.
[39] M.G. Freire, S.P.M. Ventura, L.M.N.B.F. Santos, I.M. Marrucho, J.A.P. Coutinho, Fluid Phase Equilib. 268 (2008) 74–84.
[40] M.J. Frisch, G.W. Trucks, H.B. Schlegel, G.E. Scuseria, M.A. Robb, J.R. Cheeseman, G. Scalmani, J.A. Montgomery Jr., T. Vreven, K.N. Kudin, J.C. Burant, J.M. Millam, S.S. Iyengar, J. Tomasi, V. Barone, B. Mennucci, M. Cossi, G. Scalmani, N. Rega, G.A. Petersson, H. Nakatsuji, M. Hada, M. Ehara, K. Toyota, R. Fukuda, J. Hasegawa, M. Ishida, T. Nakajima, Y. Honda, O. Kitao, H. Nakai, M. Klene, X. Li, J.E. Knox, H.P. Hratchian, J.B. Cross, V. Bakken, C. Adamo, J. Jaramillo, R. Gomperts, R.E. Stratmann, O. Yazyev, A.J. Austin, R. Cammi, C. Pomelli, J.W. Ochterski, P.Y. Ayala, K. Morokuma, G.A. Voth, P. Salvador, J.J. Dannenberg, V.G. Zakrzewski, S. Dapprich, A.D. Daniels, M.C. Strain, O. Farkas, D.K. Malick, A.D. Rabuck, K. Raghavachari, J.B. Foresman, J.V. Ortiz, Q. Cui, A.G. Baboul, S. Clifford, J. Cioslowski, B.B. Stefanov, G. Liu, A. Liashenko, P. Piskorz, I. Komaromi, R.L. Martin, D.J. Fox, T. Keith, M.A. Al-Laham, C.Y. Peng, A. Nanayakkara, M. Challacombe, P.M.W. Gill, W. Johnson, W. Chen, M.W. Wong, C. Gonzalez, J.A. Pople, Gaussian 03, Revision D.02, 2004. (Wallingford, CT).

[41] C.-M. Hsieh, S.I. Sandler, S.-T. Lin, Fluid Phase Equilib. 297 (2010) 90–97.
[42] E. Androulaki, N. Vergadou, J. Ramos, I.G. Economou, Mol. Phys. 110 (2012) 1139–1152.
[43] L. Crowhurst, P.R. Mawdsley, J.M. Perez-Arlandis, P.A. Salter, T. Welton, Phys. Chem. Chem. Phys. 5 (2003) 2790–2794.
[44] J.L. Anderson, J. Ding, T. Welton, D.W. Armstrong, J. Am. Chem. Soc. 124 (2002) 14247–14254.
[45] K.A. Kurnia, S.P. Pinho, J.A.P. Coutinho, Ind. Eng. Chem. Res. 53 (2014) 12466–12475.
[46] K. Dong, S. Zhang, D. Wang, X. Yao, J. Phys. Chem. A 110 (2006) 9775–9782.
[47] P.A. Hunt, I.R. Gould, J. Phys. Chem. A 110 (2006) 2269–2282.
[48] M. Bühl, A. Chaumont, R. Schurhammer, G. Wipff, J. Phys. Chem. B 109 (2005) 18591–18599.
[49] T. Cremer, C. Kolbeck, K.R.J. Lovelock, N. Paape, R. Wölfel, P.S. Schulz, P. Wasserscheid, H. Weber, J. Thar, B. Kirchner, F. Maier, H.-P. Steinrück, Chem. Eur. J. 16 (2010) 9018–9033.